Superscattering engineering through combined resonant modes

Yongge Wang[1], Xin Ye[1], Jingfeng Yao[1,2,3,‡], Ying Wang[1,2,3], Chengxun Yuan[1,2,3,§], Zhongxiang Zhou[1,2,3,‖]

[1]School of Physics, Harbin Institute of Technology, Harbin 150001, People's Republic of China
[2] Heilongjiang Provincial Key Laboratory of Plasma Physics and Application Technology, Harbin 150001, People's Republic of China
[3] Heilongjiang Provincial Innovation Research Center for Plasma Physics and Application Technology, Harbin 150001, People's Republic of China

Abstract. A sub-wavelength particle with a total scattering cross section that exceeds the single channel limit is referred to as a superscatterer, which can provide ability to control light in nanoscale. A variety of superscatter structures have been suggested, most of them are typically constructed with strong forward scattering but minor backscattering. This unusual behavior can be attributed to the superposition of resonant modes in adjacent angular momentum channels. We reveal the mechanism of super backscattering for subwavelength column, which can be formed by recombining non-adjacent resonant modes, as confirmed by our numerical analysis.

Keywords: Superscattering, Light scattering, Light-matter interaction
Submitted to: *J. Phys. D: Appl. Phys.*

‡ yaojf@hit.edu.cn
§ yuancx@hit.edu.cn
‖ zhouzx@hit.edu.cn

1. Introduction

The scattering of light by small particles is a fundamental problem in modern optics, dating back to Rayleigh's work on atmospheric scattering.[1,2] The strength of the light-matter interaction is usually characterized by the scattering cross section. In general, small particles respond weakly to electromagnetic waves in the long-wave limit, possessing a scattering cross section proportional to λ^{-4}, where λ is the wavelength.[3] Thus enhanced light-matter interactions are desired for a variety of sub-wavelength photonics applications, such as imaging,[4,5] sensing,[6,7] heat transfer,[8] etc. Fortunately, a small object can produce a large optical response far in excess of Rayleigh scattering when resonant scattering occurs, for which it tends to exhibit a total scattering cross section that does not exceed the single-channel limit. A sub-wavelength particle with a total scattering cross section that exceeds the single channel limit is referred to as superscatterer,[9,10] implying stronger light-matter coupling, and has attracted immense attention due to its considerable potential of controlling light.

Superscattering engineering, which optimizes the maximum scattering cross section by designing the particle structure while preserving energy conservation and central symmetry, has been experimentally realized in various of systems such as microwaves,[11] acoustic waves,[12] and water waves[13] since its introduction. However, the development of superscattering focuses on the enhancement of the total scattering cross section while ignoring other scattering characteristics. Recently, various of structures for superscatterer have been proposed,[11,14–16] but most of which are typically constructed with negligible backscattering, in sharp contrast to its significant forward scattering, which limits further applications. The mainly proven capability of superscatterer is protecting the objects behind it off scattering.[13]

Backscattering is an important property used to characterize the electromagnetic properties of objects and is particularly concerned in the fields of antennas, radar, communication, sensing, etc.[17–19] Various retroreflective structures have been designed to have strong angle-insensitive backscattering capabilities such as corner reflectors, Luneberg lenses and metasurface,[20,21] which are used for a variety of applications such as radar targets or communication antennas in different fields. However, these structures usually have bulky over-wavelength profiles and cannot operate at sub-wavelengths. Therefore, the development of a sub-wavelength retroreflector based on the super-scattering mechanism will pave the way for the realization of flexible scattering feature engineering as well as high-sensitivity sensing.

The implementation of strong backscattering through the design of scatterers has recently been discussed. For instance, dielectric shell structures are used to enhance backward scattering in some previous works, which is achieved by combining an electric and a magnetic multipole resonance.[22–24] However, this method is limited to the combination of two modes and fails in the two-dimensional case.

In this work, we reexamine this ignored phenomenon in a 2D rotational symmetric superscattering system and find that this unusual behavior can be attributed to the superposition of resonant modes in adjacent angular momentum channels. In the process, we outline a general perspective on the inherent relationship between the forward and backward scattering and mode combinations and confirm that the presently designed superscatterrs exhibit trivial backscattering characteristics. We show that backscattering can be enhanced in quadratic form depending on the number of properly overlapped modes, and it can be shown that backward scattering is maximized for a given number of resonant modes. In principle, arbitrarily large backscattering can be achieved depending on the specific design of the superscatterer. Specifically, we will demonstrate enhancing backscatter beyond the reach of single channel by combining three nonadjacent resonant modes in a simple model, i.e., super backscattering.

2. Theory

In this study, the two-dimensional case of scatterers with rotational symmetry is investigated, which can be analyzed using the Mie scattering theory.[3] When a H-polarized plane wave (with the magnetic field only along the z direction) of angular frequency ω incident upon an obstacle located at the origin, the total magnetic field in the air region can be expressed in polar coordinates (r, φ) as[9,25]

$$H_z = H_0 \sum_m \left[\mathrm{i}^m \mathrm{J}_m(kr) + \mathrm{i}^m S_m \mathrm{H}_m^{(1)}(kr) \right] \mathrm{e}^{\mathrm{i}m\varphi}, \qquad (1)$$

where the time dependence is considered as $\exp(-\mathrm{i}\omega t)$. The first term in above formula refers to the incident field, where k is the wave number in the air. Here $\mathrm{J}_m(kr)$ is the m-order Bessel function of the first kind, $\mathrm{H}_m^{(1)}(kr)$ is the m-order Hankel function of the first kind, and the scattering coefficient S_m corresponds to the strength of the scattered field in the m-th angular momentum channel. H_0 is the amplitude of incident wave.

Using the definition of the cylinder function, equation (1) can be reformulated as

$$H_z = H_0 \sum_m \left[\frac{\mathrm{i}^m}{2} \mathrm{H}_m^{(2)}(kr) + \frac{1+2S_m}{2} \mathrm{i}^m \mathrm{H}_m^{(1)}(kr) \right] \mathrm{e}^{\mathrm{i}m\varphi}. \qquad (2)$$

Note that the incoming wave in the m-th channel is represented by $\frac{\mathrm{i}^m}{2}\mathrm{H}_m^{(2)}(kr)$, while the outgoing wave becomes $\frac{1+2S_m}{2}\mathrm{i}^m\mathrm{H}_m^{(1)}(kr)$. Thus, the range of S_m is restricted by the conservation of energy and angular momentum, namely $\left|\frac{1+2S_m}{2}\right| \leq \left|\frac{1}{2}\right|$ (as indicated in figure 1). The equal sign here holds when the material is lossless.

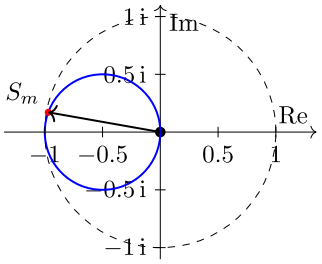

Figure 1. The value of S_m in the complex plane. The blue circle represents the trajectory of S_m (marked in red dot).

For such a scatterer, the total scattering cross section can be expressed in terms of S_m:

$$Q_{\mathrm{sc}} = \frac{2\lambda}{\pi}\sum_m |S_m|^2, \tag{3}$$

with a maximum scattering cross section in m-th channel when $S_m = -1$. In fact, it can be verified that this corresponds to the bound state of the system. Furthermore, the differential scattering cross section is given by

$$\sigma(\varphi) = \frac{\lambda}{2\pi}\lim_{r\to\infty} kr\left|\sum_m \mathrm{i}^m S_m \mathrm{H}_m^{(1)}(kr)\mathrm{e}^{\mathrm{i}m\varphi}\right|^2, \tag{4}$$

with $\sigma(0)$ and $\sigma(\pi)$ corresponding to forward and backward scattering, respectively. With the well-known asymptotic formula $\mathrm{H}_m^{(1)}(x) \sim \sqrt{\frac{2}{\pi x}}\mathrm{e}^{\mathrm{i}(x-m\pi/2-\pi/4)}$ at $x\to\infty$, $\sigma(\varphi)$ becomes

$$\sigma(\varphi) = \frac{\lambda}{\pi^2}\left|\sum_m S_m \mathrm{e}^{\mathrm{i}m\varphi}\right|^2. \tag{5}$$

Generally, in subwavelength objects, the angular momentum channels without resonance has a really small contribution to the scattering cross section. Meanwhile, apart from the fact that dipole moments are more easily induced by external fields for $m = 1$, higher order resonant modes only exhibit a significantly narrow linewidth. As a consequence, $S_m = -1$ only occurs at resonance in subwavelength system, while S_m rapidly approaches zero and negligibly contributes to $\sigma(\varphi)$ when detuning. Hence equation (5) can be simplified as $\sigma(0) \approx \frac{\lambda}{\pi^2}\sum_n 1$ and $\sigma(\pi) \approx \frac{\lambda}{\pi^2}\left|\sum_n(-1)^n\right|^2$ for forward and backward scattering, respectively, where n takes only the resonant modes. Furthermore, it is noted that the total scattering cross-section can be estimated using forward scattering for subwavelength superscatterers: $Q_{\mathrm{sc}} \approx 2\sqrt{\lambda\sigma(0)}$, implying a positive correlation. As a result, when different resonant modes of the superscatterer are combined with each other, forward scattering is always enhanced, while backward scattering presents a cancellation for the case of two adjacent channels overlap. Thus, it is again verified that the previously constructed superscatterer by sequential resonance mode superposition has a trivial backscattering property not exceeding that of the unusual scatterer. In the other hand, super backscattering can be achieved through superposition of modes where m is odd (even) with a backscattering cross section proportional to the square of the number of participating modes. This approach allows the backward scattering to be significantly enhanced without altering the forward and total scattering cross sections.

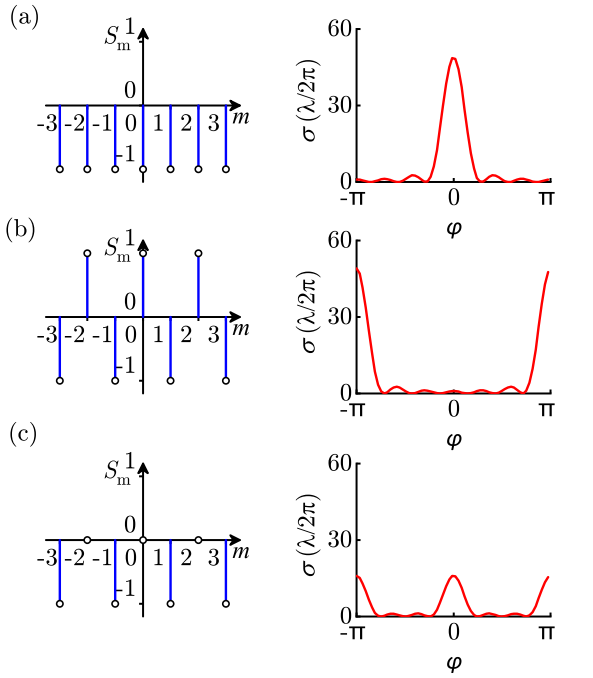

Figure 2. Relationship between the value of the scattering coefficient and the angular distribution of scattering. (a) Maximum forward scattering. (b) Maximum backward scattering but physically impossible. (c) Maximum physically allowed backward scattering. An interactive version of how $\sigma(\phi)$ depends on the scattering coefficient is available as a HTML document.

In fact, equation (5) is exactly the form of a Fourier series, and its coefficient values are limited by the conservation of energy and angular momentum. Conventional superscattering studies increase the total scattering cross section by constructing resonance in a continuous angular momentum channel, which will result in a scattering angle distribution approaching a

delta function form $\delta(\varphi)$. This explains the vanishing backward scattering of the superscatterer as shown in figure 2(a). Whereas the component of backward scattering comes from the shifted delta function $\delta(\varphi-\pi)$, which can be viewed as a limit of $\sum_m \mathrm{e}^{-\mathrm{i}m\pi}\mathrm{e}^{\mathrm{i}m\varphi}$. Such a series of the scattering coefficient gives strong backward scattering as shown in figure 2(b), but is physically impossible. To conform to the range of scattering coefficients, the series $\mathrm{e}^{-\mathrm{i}m\pi}$ are shifted and scaled to transform into the circle in the complex plane as $S_m = \frac{1}{2}\mathrm{e}^{-\mathrm{i}m\pi} - \frac{1}{2}$, obtaining maximum backward scattering in a finite angular momentum channel (figure 2(c)). Note that this is consistent with the scattering coefficient obtained from the previous derivation, providing a maximum backward scattering in the finite resonant angular momentum channel. The latter term in the scattering coefficient comes from translation in the complex plane, which contributes a forward scattering cross section comparable to the backward scattering. Consequently, there is a trade-off between the back-to-front ratio and the backward scattering cross section of the superscatterer.

3. Model and Results

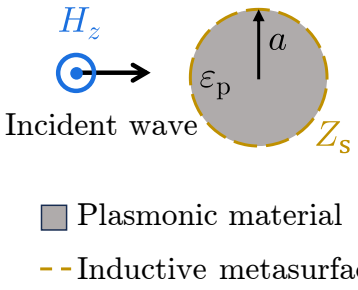

Figure 3. Schematic of H-polarized plane waves impinges on the nanorod. The scatterer is a plasmonic column with a relative permittivity of ε_p and a radius a, covered by a inductive metasurface with impedance Z_s.

Due to the tendency of resonant modes in high angular momentum channels to obtain higher eigenfrequencies, the difficulty of super backscattering is to combine non-adjacent modes while avoiding overlapping intermediate modes. Here, we introduce a minimal model to illustrate the procedure of maximizing backscatter. The structure is sketched in the figure 3, which is a plasmonic nanorod with a radius a, covered by a inductive metasurface with surface impedance quantified by Z_s. Here the relative permittivity of the plasmonic material is described by the Drude model written as $\varepsilon_\mathrm{p} = (1-\omega_\mathrm{p}^2/\omega^2)$, where ω_p is the plasma frequency. The boundary conditions thus are modified as follows:

$$H_z(r)|_{r=a^+} - H_z(r)|_{r=a^-} = -\frac{E_\varphi(r)}{Z_\mathrm{s}}|_{r=a^+}, \tag{6}$$

$$E_\varphi(r)|_{r=a^+} = E_\varphi(r)|_{r=a^-}. \tag{7}$$

In fact, the bound state of the scatterer originates from the surface plasma wave.[26] Therefore, the interface impedance changes the energy-momentum dispersion of the surface wave, and thus the resonant frequency. To illustrate this correlation, the modified surface waves dispersion relation (blue solid lines) and corresponding structural resonance (red dots for frequency and dark blue bars for linewidth) of plasmonic nanorod covered with a metasurface are shown in figure 4, where the plasma frequency is selected as $\omega_\mathrm{p} = 0.5c/a$. Here $k_\parallel$ is the surface wave propagation constant at the interface. One can observe that the resonant frequencies is exactly the eigenmodes where $k_\parallel$ in the photonic band is an integer multiple of a^{-1}. For contrast, the primary dispersion relationship of the plasma-air interface is also depicted in figure 4 as orange dashed line. It can be shown that inductive surface impedance ($\mathrm{Im}(Z_\mathrm{s}) > 0$) suppresses the frequency of plasma surface waves at higher transverse wave numbers, resulting in overlapping resonant peaks, which is also the case for the covering of a thin dielectric layer.

The extremely narrow linewidth can also be seen in figure 4(b), which illustrates the variation of $|S_m|^2$ with frequency corresponding to different m, guaranteeing a negligible contribution from the angular momentum channel deviating from resonance. In this model, the resonance modes in different angular momentum channels exhibit distinct radial profile. The higher order modes undergo more pronounced perturbation and frequency reduction, owing to their stronger localization at the interface. This leads to the establishment of a non-monotonic surface wave dispersion relation, which enables superimposition of non-adjacent modes without experiencing interference from intermediate mode.

To further demonstrate the interplay between backscattering and mode superposition, we constructed two scatterers by altering different surface impedance. The impedance of the metasurface is set as $Z_\mathrm{s} = 102\,\mathrm{i}Z_0$ in figure 4(a), leading to superscattering at frequency $\omega = 0.34492\,c/a$ by superposition of $m = \pm1, \pm2, \pm3$ modes. Here, Z_0 is the wave impedance in the free space. In contrast, superscattering involving angular momentum channels of $m = \pm1, \pm3, \pm5$ at a frequency of about $\omega = 0.35076\,c/a$ with a surface impedance of $Z_\mathrm{s} = 533.5\,\mathrm{i}Z_0$ is shown in figure 4(c). The far-field scattering patterns of these two different superscatterers are shown in figure 5. Both two superscatterers exhibit similar total scattering section, but show a dramatic difference in backward scattering. Although due to the slight deviation between dipole modes and other modes, as shown in figures 4(b) and 4(d), the scattering cross section blow the ideal case,

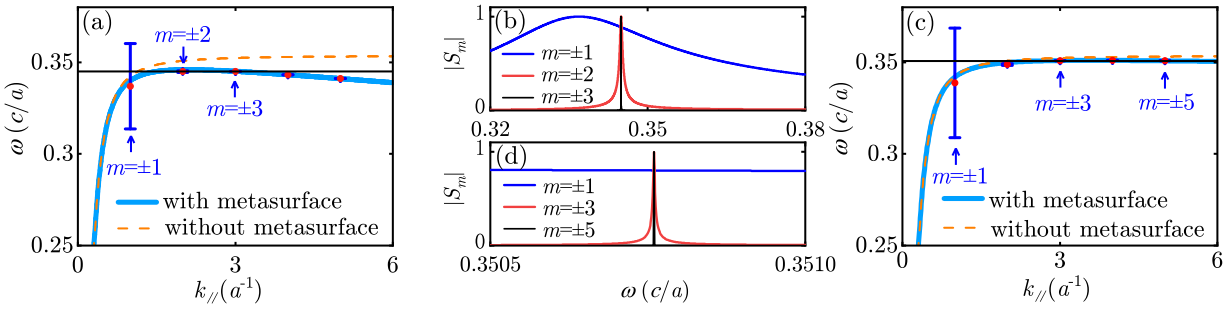

Figure 4. Manipulate the resonant frequency through the dispersion relation of surface waves. (a) The influence of inductive metasurface on the dispersion relation of surface waves and the corresponding structural resonant frequency, where the metasurface provides a surface impedance of $Z_s = 102iZ_0$. Resonance occurs when the surface wave propagation constant $k_{\parallel}$ is an integer multiple of a^{-1}, and the red dots and the bars correspond to the resonant frequency and the linewidth, respectively. The black line emphasizes the frequency at which superscattering occurs ($\omega = 0.34492\,c/a$), and the modes involved in the superposition are indicated by arrows. And (b) shows the scattering coefficients from individual channels. (c) Same as (a), but with the surface impedance tuned to $Z_s = 533.5\,iZ_0$ and superscattering achieved by superposition of modes with $m = \pm1, \pm3, \pm5$ instead. The superscattering in (c) presents at a frequency about $\omega = 0.35076\,c/a$. (d) The scattering coefficients corresponds to the case in (c).

the aforementioned influence of mode superposition on backscattering is still valid. In figure 5(a), the $m = \pm2$ and $m = \pm3$ channels cancel out for forward scattering, leaving only the contribution of the $m = \pm1$ mode, resulting in a scattering cross section $\sigma(0)$ of about $4\lambda/\pi^2$. For the case of odd mode superposition, as shown in figure 5(b), as expected, it is observed that backscattering appears to be enhanced as much as forward scattering, suggesting super backscattering. Backward scattering in this case reaches 29.43 times the single-channel scattering limit (ideally up to 36 times), and 7.35 times the strongest backward scattering in ordinary superscatterers. In addition, we calculated that $Q_{sc} = 5.60(2\lambda/\pi) \approx 2\sqrt{\lambda\sigma(0)} = 5.63(2\lambda/\pi)$ for figure 5(a), and $Q_{sc} = 5.34(2\lambda/\pi) \approx 2\sqrt{\lambda\sigma(0)} = 5.42(2\lambda/\pi)$ for figure 5(b), verifying the correlation between the total scattering cross-section and the forward scattering cross-section.

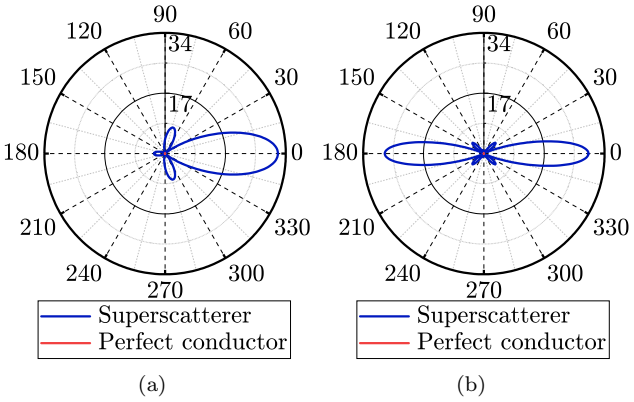

Figure 5. Far-field scattering patterns of two different superscatterers compared to a perfect electrical conductor (red line). The radial length represents the magnitude of cross section per azimuthal angle, which is in unit of λ/π^2. Both two superscatterers exhibit similar forward scattering, but dramatically different backward scattering. (a) The blue curve depicts the scattering pattern of superscatterer at a frequency of $\omega = 0.34492\,c/a$, which is composed of $m = \pm1, \pm2, \pm3$ resonance modes, corresponding to the condition in figure 4(a). (b) The combination of $m = \pm1, \pm3, \pm5$ angular momentum channels corresponds to the situation in figure 4(c). The working frequency is about $\omega = 0.35076\,c/a$.

In fact, there is no theoretical limitation preventing further superposition of modes to continue improving reflectivity. For a multi-channel resonant degenerate scatterer, the radial field distributions of the individual modes are different. Thus, through the design of radial material parameter distributions, different modes can be perturbed differently, resulting in a specific modes combination design. However, the sensitivity of parameter perturbations and losses may make make it difficult to assemble such scatterers with highly degenerate modes. Therefore, exploring the use of low-loss artificial materials such as spoof surface plasmon,[27,28] additional resonance mechanisms such as phonon polariton,[29] and anisotropic materials such as hyperbolic media will be the future research direction of superscattering.[15,16]

The near-field distribution of scattering problems provides another perspective, as presented in figure 6. The field strength distribution in the near-field region does not exhibit the same scattering angle distribution characteristics as the far field. Typical superscatters commonly create large shadow behind the structure, and the shadow is much larger that the physical size of the particle, consistent with Figs. 6(a) and 6(b). Therefore, the superscatter is capable of protecting the objects behind it against scattering. This is due to the fact that the forward-scattered wave coherently cancels with the incident plane wave at a few wavelengths from the scatterer. However, forward scattering does not

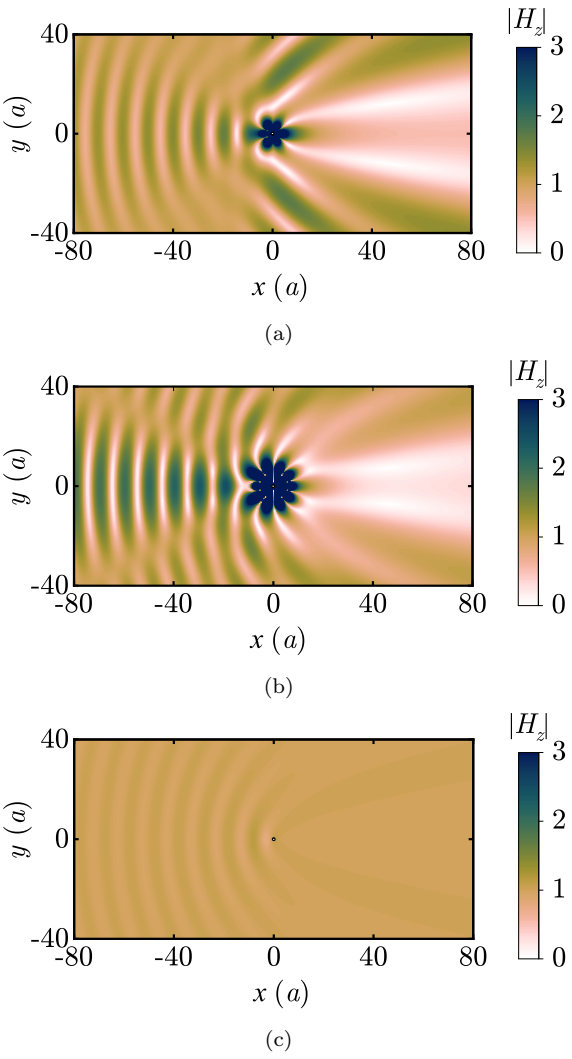

Figure 6. $|H_z|$ profile of plane waves incident from the left to three different scatterers, which is normalized by the amplitude of the incident wave. (a) Typical superscatter with $m = \pm1, \pm2, \pm3$ modes superposition, as depicted in figure 4(a). (b) Superscatter with strong backscattering, for the combination of $m = \pm1, \pm3, \pm5$ modes, corresponds to the situation in figure 4(c). (c) The perfect electrical conductor acts as a scatterer.

contribute to the focusing of electromagnetic waves. This is enabled by super backscattering as shown in figure 6(b), where the reflection and incident waves are enhanced by superposition, hence more versatile application potential.

4. Conclusion

In summary, in subwavelength superscatterers, only the angular momentum channel supporting the resonance contributes to the scattering cross section, so we can analyze the directionality of such a system. We found a positive correlation between forward scattering and total scattering cross section, implying the contribution of any resonance modes will enhance forward scattering. As a contrast, backscattering cancels out in the superposition of resonant modes of adjacent angular momentum channels. To overcome this, we revealed that backscattering can be enhanced by artificially selecting odd (even) angular momentum resonance for superposition without changing the total scattering cross section, yielding a new degree of freedom in the design of scattering properties. A considerable strong backscattering exceeding the single-channel limit was achieved by combining non-adjacent modes induced by the specifically designed non-monotonic dispersion of surface waves, verifying the validity of the method. Also, this can be further enhanced in quadratic form depending on the number of overlapping modes through a particular design.

Furthermore, it should be noted that there are works that have implemented superscattering in other ways.[30,31] These explorations have expanded the original definition of superscattering, resulting in the disruption of rotational symmetry or energy conservation, making it possible to achieve super backscattering under specific conditions. Moreover, it is well known that the subwavelength antennas with specific designs can exhibit strong backscattering, but only works for incoming waves in specific directions to the distortion of rotational symmetry. Our approach is based on rigorous analysis when angular momentum and energy conservation, providing an isotropic strong backscattering. In general, this method is also effective for other structures with rotational symmetry. Our work not only offers a deeper perspective for the fundamental understanding of electromagnetic superscattering, but also provides a concrete route to control scattering characteristics for potential applications in nanoscale.

Acknowledgments

This work is supported by the National Natural Science Foundation of China (NSFC, No. 12205067, No. 12375199 and No. 12175050).

[1] Rayleigh L 1871 *Phil Mag* **41** 107–120
[2] Rayleigh L 1871 *Phil Mag* **41** 274–279
[3] Jackson J D 1999 *Classical electrodynamics* 3rd ed (New York: Wiley) ISBN 978-0-471-30932-1
[4] Alfaro-Mozaz F, Alonso-González P, Vélez S, Dolado I, Autore M, Mastel S, Casanova F, Hueso L, Li P, Nikitin A Y *et al.* 2017 *Nature communications* **8** 15624
[5] Padilla W J and Averitt R D 2022 *Nature Reviews Physics* **4** 85–100
[6] Altug H, Oh S H, Maier S A and Homola J 2022 *Nature nanotechnology* **17** 5–16
[7] Aigner A, Tittl A, Wang J, Weber T, Kivshar Y, Maier S A and Ren H 2022 *Science advances* **8** eadd4816

[8] Salihoglu H, Shi J, Li Z, Wang Z, Luo X, Bondarev I, Biehs S A and Shen S 2023 *Physical Review Letters* **131** 086901
[9] Ruan Z and Fan S 2010 *Physical review letters* **105** 013901
[10] Ruan Z and Fan S 2011 *Applied Physics Letters* **98**
[11] Qian C, Lin X, Yang Y, Xiong X, Wang H, Li E, Kaminer I, Zhang B and Chen H 2019 *Physical review letters* **122** 063901
[12] Lee T, Nomura T, Schmalenberg P, Dede E M and Iizuka H 2019 *Phys. Rev. Appl.* **12**(5) 054059
[13] Qin Z, Qian C, Shen L, Wang X, Kaminer I, Chen H and Wang H 2023 *National Science Review* **10** nwac255
[14] Mirzaei A, Miroshnichenko A E, Shadrivov I V and Kivshar Y S 2014 *Applied Physics Letters* **105**
[15] Kumar R and Kajikawa K 2020 *Optics Express* **28** 1507–1517
[16] Qian C, Lin X, Yang Y, Gao F, Shen Y, Lopez J, Kaminer I, Zhang B, Li E, Soljacic M *et al.* 2018 *Acs Photonics* **5** 1506–1511
[17] Wang S, Chen K S and Sato M 2021 *IEEE Journal of Selected Topics in Applied Earth Observations and Remote Sensing* **14** 440–451
[18] Feng M, Li Y, Zhang J, Han Y, Wang J, Ma H and Qu S 2018 *Applied Physics Letters* **113** 143504 ISSN 0003-6951
[19] Hao J, Wang X, Yang S and Gao H 2023 *Applied Sciences* **13** ISSN 2076-3417
[20] Díaz-Rubio A, Asadchy V S, Elsakka A and Tretyakov S A 2017 *Science Advances* **3** e1602714
[21] Arbabi A, Arbabi E, Horie Y, Kamali S M and Faraon A 2017 *Nature Photonics* **11** 415+
[22] Liberal I, Ederra I, Gonzalo R and Ziolkowski R W 2015 *Journal of Optics* **17** 072001
[23] Powell A W, Hibbins A P and Sambles J R 2021 *Applied Physics Letters* **118**
[24] Powell A W, Mrnka M, Hibbins A P and Sambles J R 2022 *Photonics* **9** 6
[25] Ye X, Wang Y, Yao J, Yuan C, Zhou Z, Astafiev A M and Kudryavtsev A A 2022 *Journal of Physics D: Applied Physics* **55** 345201
[26] Ye X, Wang Y, Yao J, Wang Y, Yuan C and Zhou Z 2023 *Physical Review B* **107** 195301
[27] Wu H W, Fang Y, Quan J Q, Han Y Z, Yin Y Q, Li Y and Sheng Z Q 2019 *Physical Review B* **100** 235443
[28] Shcherbinin V I, Fesenko V I, Tkachova T I and Tuz V R 2020 *Physical Review Applied* **13** 024081
[29] Chern R L, Chang C C and Chang C C 2006 *Physical Review B* **73** 235123
[30] Shamkhi H, Kupriianov A, Weiss T, Pavlov A, Redka D, Bobrovs V, Kivshar Y, Shalin A *et al.* 2023 *Nature Communications* **14** 4689–4689
[31] Qian C, Yang Y, Hua Y, Wang C, Lin X, Cai T, Ye D, Li E, Kaminer I and Chen H 2022 *Nature communications* **13** 4383